Flame Spreading and Ignition Transients in Solid Grain Propellants

S. DESOTO* AND H. A. FRIEDMAN†
North-American Aviation, Inc., Canoga Park, Calif.

An analysis of grain ignition and flame spreading in solid-propellant rocket engines was performed to calculate chamber pressure as a function of time during this phase. Assumed for the analysis were isothermal one-dimensional gas flow in the chamber, spatially uniform gas pressure, two-dimensional transient heat conduction in the grain, perfect gas properties, choked nozzle flow, and gas generation due only to grain surface deflagration. Also investigated is the case of a diaphragm stretched across the throat entrance which bursts with sufficient pressure build-up. Initial conditions include instantaneous gasless ignition of a section of the upstream end of the grain, uniform pressure and temperature in the gas, a uniformly distributed temperature in the unignited portion of the grain, and an axially varying gas velocity distribution. A quasi-analytic solution (analytic in each time step) for chamber pressure is coupled, through changes in the burning wall area, to a finite difference solution for grain temperature (using the stable Peaceman-Rachford alternating direction method). After the end of flame spreading, the pressure calculation alone is continued until steady-state conditions are approximated. A computer program was written to perform the calculating for varying input data.

Nomenclature

a', b', c' = constants in expression for $h(x, \tau)$ which depend on the nature of the boundary-layer flow
a, b, c = constants in $h(x, \tau)$ depending on the heat-transfer effects
A_g = (constant) flow cross-sectional area of combustion chamber
$A_w(x, \tau)$ = burning area of solid grain surface upstream of the position x
$\bar{A}_w(\tau)$ = total burning area of grain surface [$\bar{A}_w(\tau) = A_w(\sigma, \tau)$]
$\bar{A}_{w,\nu}$ = numerically obtained sequence of values approximating the sequence $\bar{A}_w(\tau_\nu)$, $\nu = 0, 1, \ldots$
$A_{w,\max}$ = maximum value of A_w[$A_{w,\max} = A_w(L, \tau)$ for $\tau \geq \tau_L$]
A^* = (constant) cross-sectional area at the nozzle throat
C_D = nozzle discharge coefficient
$c_{p,g}$ = specific heat at constant pressure of the gaseous products
c_w = specific heat of the grain
d = "pipe" (chamber) diameter
F, N_ν = abbreviations given in Eqs. (15) and (16)
g = acceleration due to gravity
$h(x, \tau)$ = effective heat-transfer coefficient
$h_\nu(x)$ = sequence of functions approximating $h(x, \tau_\nu)$; $\nu = 0, 1, \ldots$
K, s = (constant) coefficient and exponent in expression for grain surface recession rate which are characteristic of the propellant used, $s < 1$
k_g = thermal conductivity of the gaseous products
$k_{w,a}$ = constant thermal conductivity of the grain in the axial x direction
$k_{w,b}$ = constant thermal conductivity of the grain in the radial y direction
L = total (axial) length of the grain
L_c = "starting length" of the chamber
M' = abbreviation for const $C_D(\gamma g/R)^{1/2} \times [2/(\gamma+1)]^{(\gamma+1)/2(\gamma-1)}$
m = effective molecular weight of propellant gases
Nu = Nusselt number
P_{amb} = ambient pressure
$P_g(\tau)$ = equilibrium pressure of the gaseous products in the chamber
$P_{g,\nu}$ = sequence of values approximating $P_g(\tau_\nu)$, $\nu = 0, 1, \ldots$
$P_{g,f}$ = steady-state value of P_g
P_I = initial gas pressure, $P_I = P_g(0)$
$P_0(\tau)$ = stagnation pressure of the gases
R = gas constant
$Re(x, \tau)$ = Reynolds number equal to $\rho_g x u_g/\mu$
$Re_D(x, \tau)$ = Reynolds number based on "pipe" diameter and equal to $\rho_g d u_g/\mu$
$T(x, y, \tau)$ = solid grain temperature
T_g = (constant) freestream temperature of the gases in the chamber
T_{ig} = igniton temperature of solid grain
T_I = initial temperature of solid grain
T_0 = stagnation temperature of the gases
$u_g(x, \tau)$ = freestream gas velocity in the chamber
$u_{g\nu}(x)$ = approximation to $u_g(x, \tau_\nu)$, $\nu = 0, 1, \ldots$
$\bar{V}$ = total chamber gas volume
$V(x)$ = gas volume upstream of the position x, thus $\bar{V} = V(L)$
$W_g(x, \tau)$ = mass flow rate of gas past the axial position x
$W_{ig}(\tau)$ = mass flow rate of gas produced by the igniter
$W_n(\tau)$ = mass flow rate of gas through the nozzle from the chamber
$\bar{W}_w(\tau)$ = mass flow rate of gas generated by the entire burning portion of the grain
$W_w(x, \tau)$ = mass flow rate of gas generated by the grain upstream of x, thus $\bar{W}(\tau) = W(\sigma, \tau)$
$W_{n,f}$ = value of W_n at $\tau = \tau_f$
$\bar{W}_{w,f}$ = value of $\bar{W}_w$ at $\tau = \tau_f$
x = distance measured along the axis of symmetry from the upstream end of the grain
y = distance into the grain in a direction normal to the grain surface (this will be called the "radial" direction)
α_a, α_b = thermal diffusivities of solid grain in the x and y directions, respectively
β = constant ratio of wall area to axial length equal to $\bar{A}_w/\dot{\sigma}$
γ = ratio of specific heats of the gas

Presented as Preprint 64-122 at the AIAA Solid Propellant Rocket Conference, Palo-Alto, Calif., January 29–31, 1964; revision received October 19, 1964. The research reported herein was conducted under North American Aviation Study Authorization No. 6051-0019 and No. 6031-0005. The authors wish to acknowledge the helpful assistance rendered by Martin Summerfield, Princeton University and Rocketdyne Consultant, in the early stages of their work.

* Senior Technical Specialist, Mathematics and Statistics Group, Research Department, Rocketdyne Division. Member AIAA.

† Senior Research Engineer, Mathematics and Statistics Group, Research Department, Rocketdyne Division.

δ = thickness of grain in y direction
μ = viscosity of the gaseous products in the chamber
$\rho_g(\tau)$ = density of the gases in the chamber
$\rho_{g,\nu}$ = approximation to $\rho_g(\tau_\nu)$, $\nu = 0, 1, 2, \ldots$
ρ_w = density of the grain
$\sigma(\tau)$ = burning length of the grain, i.e., axial position of the flame front
σ_ν = approximation to $\sigma(\tau_\nu)_g$, $\nu = 0, 1, \ldots$
τ = time
$\Delta\tau$ = time increment
τ_L = time at which flame spreading ends; i.e., when $\sigma = L$
τ_f = time at which P_g reaches its steady-state value $P_{g,f}$
τ_ν = νth discretely spaced instant in time, $\tau_\nu = \nu\Delta\tau$, for $\nu = 0, 1, \ldots$
ψ = temperature and pressure dependent term of $h(x, \tau)$ explained following Eq. (40)
χ = $x - \sigma$

Subscripts

a, b = material properties in the x and y directions, respectively
f = steady-state conditions
g = property of the gaseous products in the chamber or of the gaseous portion of the chamber
I = initial conditions, $\tau = 0$
L = conditions at the end of the grain or conditions surrounding the end of flame spreading
0 = stagnation conditions of the gas
w = properties of the solid propellant grain
ν = index for discretizing the continuous variable τ

Introductory Considerations

THE actual physical phenomena occurring during the flame-spreading period in solid-propellant rocket motors are exceedingly difficult to analyze in an exact fashion. Thus, a somewhat simplified mathematical model has been developed which represents an appropriate first step in an attempt to obtain the pressure response in a solid-propellant rocket motor. In any such analysis, it is necessary to describe the flame-spreading process that occurs during the initial phases of the transient period. The flame-spreading rate depends on heat-transfer effects from the hot gases produced by the grain itself and the igniter (unless a gasless igniter is employed). When strong shock waves exist during the ignition transient, they in turn influence the heat-transfer effects.

During the ignition phase of a solid-propellant rocket engine, the flow rate of combustion gases entering the chamber depends on the gaseous igniter characteristics, the properties of the grain, the pressure already existing in the chamber, and the amount of grain surface area already burning. In particular, the gas-generation rate of the grain increases with chamber pressure and with the burning area of the grain. If a nozzle diaphragm is used to seal the chamber, the rate of pressure increase simply depends on the gas-generation rate and the chamber volume. If no nozzle diaphragm is used, however, the pressure rate is affected also by the rate of gas efflux through the rocket nozzle. Immediately after the rupture of a nozzle diaphragm, the pressure will momentarily decrease when the gas-efflux rate is greater than the gas-generation rate.

In case a gasless igniter is employed (as is assumed in the present analysis), the mass balance during the ignition phase is simplified through omission of a mass flow rate term for the igniter. Moreover, since it is unlikely that strong shock waves will be produced in such a case, all rarefaction and shock effects have been neglected in the present analysis.

It was stated in the foregoing that the gas-generation rate depends, among other factors, directly on the burning area of the grain and the chamber pressure. The flame-spreading rate, however, influences the burning area of the grain, which in turn affects the rate of gas generation, and consequently the chamber pressure. Thus, there exists a "feedback" or "coupling" of the important phenomena, since the chamber pressure influences both the gas-generation rate and the heat-transfer rate to the grain, thereby affecting the flame-spreading rate. This coupling makes a purely analytic treatment of the problem difficult and suggests a basically numerical approach. After the flame has spread across the entire grain, however, heat-transfer phenomena are no longer significant and the calculation of the rate of increase of chamber pressure is no longer complicated by a changing grain burning area.

In the analysis that follows, a mathematical model is developed to describe the coupling of the pressure response to the flame-spreading rate during the ignition phase. The assumptions made in describing the physical process include 1) one-dimensional transient gas flow in the combustion chamber; 2) two-dimensional transient heat conduction in the grain; 3) holding $\bar{V}$, A_g, and T_g constant; 4) allowing P_g and ρ_g to vary only with time τ, not with axial distance x; 5) varying u_g and h with x as well as τ; 6) generation of gas only by deflagration of the grain surface; 7) negligible recession of the grain surface to estimate grain surface area (however, a rate of recession $dy/d\tau$ is assumed in order to obtain a mass flow rate from the surface); 8) applicability of the perfect gas law to all gases generated; 9) choking of the nozzle at all times during the ignition phase; and 10) no mass accumulation in the nozzle, i.e., beyond the grain end.

In addition to the mathematical model, numerical procedures used to obtain a solution are presented below, along with a discussion of results obtained using the 7094 program written to perform the calculations.

Analysis and Discussion

No Diaphragm

Pressure calculations

The pressure response within a chamber with a gas influx at one end and a gas efflux at the other end may be found by considering an appropriate mass balance. If the gas pressure and density within the chamber are assumed to be uniformly distributed at any instant of time, one may write

$$W_{ig} + \bar{W}_w = W_n + \bar{V}(d\rho_g/d\tau) \tag{1}$$

where $\bar{V}d\rho_g/d\tau$ is the rate of gas filling of the chamber. (In reality momentum considerations dictate a pressure gradient in the direction of flow, and future work including pressure gradients should be considered.)

An equation analogous to the one-dimensional continuity equation of fluid flow may be written for the receding solid grain:

$$\bar{W}_w = \rho_w \bar{A}_w(dy/d\tau) \tag{2}$$

where ρ_w is used rather than $\rho_w - \rho_g$, since $\rho_w \gg \rho_g$. Substituting in Eq. (2) the following empirical form for the burning rate of the grain as a function of pressure

$$dy/d\tau = KP_g^s \tag{3}$$

we obtain

$$\bar{W}_w = \rho_w \bar{A}_w K P_g^s \tag{4}$$

Here also future considerations should include more complete expressions than Eqs. (3) and (4).

In order to evaluate $d\rho_g/d\tau$ in Eq. (1), we assume that the gaseous combustion products follow the perfect gas law and that the gas temperature T_g remains constant both spatially and with respect to time. Thus we obtain

$$d\rho_g/d\tau = (1/RT_g)(dP_g/d\tau) \tag{5}$$

The mass flow rate W_n of a perfect gas leaving the chamber through a nozzle which is not choked is a complicated function of the nozzle pressure ratio and gas specific heats. However, in the case of isentropic flow through a converging-diverging

nozzle, the nozzle throat becomes choked when the discharge pressure of the nozzle is only slightly less than the inlet pressure. Experience indicates that this occurs almost immediately after the inception of the chamber pressure rise. After this time the mass rate of gas flow through the nozzle (out of the chamber) can be expressed by the following simple equation

$$W_n = M'A^*P_0/T_0^{1/2} \tag{6}$$

If the port area of the chamber is somewhat larger (say 50%) than the nozzle throat area, the Mach number of the gas flow in the combustion chamber is expected to be decidedly subsonic. Thus there is very little difference between the static and stagnation values of the chamber pressure and temperature, and static values may be used in Eq. (6) (the appropriate values are those existing just upstream of the nozzle). However, since we are assuming constant chamber temperature and uniformly distributed chamber pressure, we shall replace T_0 and P_0 in Eq. (10) by T_g and P_g, respectively, obtaining

$$W_n = M'A^*P_g/T_g^{1/2} \tag{7}$$

Finally, even a quasi-analytical solution of Eq. (1) would be extremely difficult with a nonzero W_{ig} term. Thus the present analysis is made assuming gasless ignition, and W_{ig} vanishes. Thus, substituting Eqs. (4, 5, and 7) in (1), there results

$$K\rho_w\bar{A}_wP_g^s = (M'A^*/T_g^{1/2})P_g + (\bar{V}/RT_g)(dP_g/d\tau) \tag{8}$$

During the ignition period, only a very thin surface layer of propellant is consumed. Hence, for all practical purposes, the chamber volume $\bar{V}$ may be considered constant, so that the only dependent variables appearing in Eq. (8) will be P_g and A_w. Nonetheless Eq. (8) is still highly nonlinear, not only because of the term P_g^s but also because $\bar{A}_w$ is a function of the dependent variable P_g. Further, the functional dependence of $\bar{A}_w$ upon P_g (and thus τ) which describes the flame spreading is unknown, being coupled to the heat-transfer phenomena mentioned in the introduction and discussed below. Consequently, a quasi-numerical treatment of Eq. (8) is indicated. We suppose that $\bar{A}_w$ is constant for sufficiently small time intervals $\Delta\tau$; that is, in each time interval $\tau_{\nu-1} < \tau < \tau_\nu$ we assign to $\bar{A}_w$ the value $\bar{A}_{w,\nu-1}$ obtained (numerically) at time $\nu_{\nu-1}$. Here τ_ν is defined by

$$\tau_\nu = \nu\Delta\tau \qquad \nu = 1, 2, \ldots \tag{9}$$

Equation (8) then becomes a sequence of Bernoulli equations (one for each value of ν) that are easily solved in each interval, yielding the following approximate sequence of values:

$$P_{g,\nu} = [N_\nu - (N_\nu - P_{g,\nu-1}{}^{1-s}) \exp\{-(1-s)F\Delta\tau\}]^{1/(1-s)} \qquad \nu = 1, 2, \ldots \tag{10}$$

where s is the constant defined by Eq. (3), and

$$F = M'A^*R(T_g)^{1/2}/V \tag{11}$$

$$N_\nu = (K\rho_w(T_g)^{1/2}/(12)(144)^sM')(\bar{A}_{w,\nu-1}/A^*) \tag{12}$$

The values of K and s defined by Eq. (3) will be given so that P_g appears in units of pounds per square inch and y in inches. However, to avoid confusion in calculating such constants as M' and R, the units of pressure will be taken everywhere as pounds per square foot and the unit of length will be expressed in feet. Thus the constant K has been divided by the term $(12)(144)^s$ in Eq. (12).

When the flame-spreading process reaches the end of the grain ($\bar{A}_w = A_{w,\max}$) then $\bar{A}_w$ may be considered constant and an analytical solution of Eq. (8) may be obtained directly.

It should be noted here that for the case of gaseous ignition, the W_{ig} term would be included in Eq. (8) and a completely numerical, rather than quasi-numerical, procedure would be employed.

It is obvious that when $\bar{W}_w > W_n$ (i.e., the gas generation rate is greater than the gas discharge rate through the nozzle) the chamber pressure should increase with time, and when $\bar{W}_w < W_n$, the chamber pressure should decrease. But from Eqs. (4) and (6), $\bar{W}_w > W_n$ implies that

$$\rho_w\bar{A}_wKP_g^s/12(144)^s > M'A^*P_g/T_g^{1/2} \tag{13}$$

or at time τ_ν

$$[\rho_wK(T_g)^{1/2}/12(144)^sM'](\bar{A}_{w,\nu-1}/A^*) > P_{g,\nu}{}^{1-s} \tag{14}$$

Combining Eqs. (12) and (14) there results

$$N_\nu > P_{g,\nu}{}^{1-s} \tag{15}$$

as the condition for increasing chamber pressure. The condition for decreasing chamber pressure is, conversely,

$$N_\nu < P_{g,\nu}{}^{1-s} \tag{16}$$

It can be seen from Eqs. (12) and (16) that the chamber pressure will decrease for sufficiently small values of $\bar{A}_{w,\nu-1}$ and sufficiently large values of $P_{g,\nu}$. This can occur physically, for example, when a diaphragm that seals the chamber bursts after a sufficiently high pressure $P_{g,\nu}$ has been generated in the chamber during a period in which the burning wall area $\bar{A}_{w,\nu-1}$ is small because of a low flame-spreading rate. Therefore, in order to prevent a "hang fire" from occurring when the inequality (16) obtains, the flame spreading should cause $\bar{A}_w$ to increase at a sufficiently high rate even if the chamber pressure is decreasing. Then the pressure will subsequently continue to decrease until such time as the inequality in Eq. (16) becomes an equality, i.e.,

$$N_\nu = P_{g,\nu}{}^{1-s} \tag{17}$$

At this point, the pressure will be at a minimum, and thereafter as $\bar{A}_{w,\nu}$ increases the physical condition expressed by Eq. (15) will hold and the chamber pressure will begin to rise.

If $A_{w,\max}$ is defined as the exposed surface area of the entire grain (i.e., the maximum burning area), then a value $N_\nu = N_{\max}$ defined by Eq. (12) may be associated with $A_{w,\max}$. As far as the ignition transient is concerned, $A_{w,\max}$ and $N_{\max}$ are constants. The "steady-state" pressure is attained when, analogous to Eq. (17), we write

$$N_{\max} = P_{g,f}{}^{1-s} \tag{18}$$

(The designation "steady state" is of course relative to our assumption of no recession of the grain surface; in reality, for large periods of time, the grain surface recedes and changes area, thereby affecting the steady-state pressure and flow rate.)

Equation (18) may also be derived directly by setting $d\rho/d\tau = 0$ in Eq. (8) and solving for $P_{g,f}{}^{1-s}$ [as well as introducing the conversion factor, $12(144)^s$].

Velocity calculations

The convective heat-transfer effects will, in general, depend on the Reynolds number Re calculated on the basis of the distance x rather than the chamber diameter. In fact, the chamber behaves like the "starting length" of a pipe, since the boundary layers at opposing points of the grain surface will most likely not meet until say 40 diam downstream from the "entrance," and consequently the chamber flow is not "fully developed." This question is discussed in more detail in the heat-transfer discussion below.

The Reynolds number includes as a factor a power of the gas velocity u_g, which can be evaluated from mass balance and momentum considerations. In the following, an approximation to this velocity will be derived making use of the assumption already given of uniformly distributed gas pressure and temperature. Using the perfect gas law, this implies that the density is uniformly distributed spatially although it does vary with time since pressure does. Using the variation

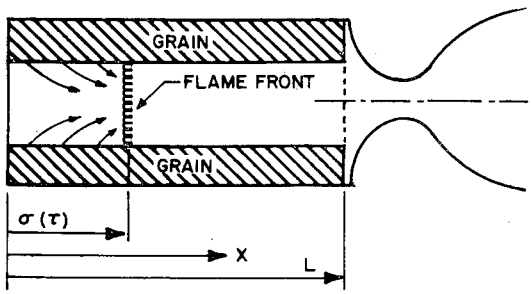

Fig. 1a Position $\sigma(\tau)$ of advancing flame front.

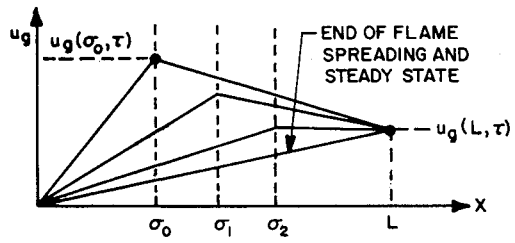

Fig. 1b Spatial distribution of u_g for several positions of σ.

of ρ_g with time, we show that the gas velocity u_g cannot be uniformly distributed during the transient period in a passage of constant cross-sectional area. This can be seen from the appropriate form of the one-dimensional continuity equation which applies only for the gas region over the unburned portion of the grain:

$$(\partial \rho_g/\partial \tau) + \rho_g(\partial u_g/\partial x) = 0$$

We see that, since $\partial \rho_g/\partial \tau \neq 0$, then $\partial u_g/\partial x \neq 0$ and hence u_g cannot be uniformly distributed. If spatial uniformity of gas pressure and temperature were not assumed, considerably more complicated techniques than those described below (such as the method of characteristics) would have to be used.

The following discussion refers to the schematic diagram shown in Fig. 1a. In order to obtain an expression for u_g, we write a mass balance similar to that given in Eq. (1) (without the $\bar{W}_{ig}$ term), but one which varies with x as well as τ (see Fig. 1):

$$W_w = W_g + V(d\rho_g/d\tau) \qquad 0 \leq x \leq L, \quad \tau > 0 \quad (19)$$

Here

W_g = the mass flow rate past the axial position x [and thus, assuming no mass accumulation in the nozzle, $W_g(L, \tau) = W_n(\tau)$]

$V d\rho_g/d\tau$ = the rate of mass accumulation in the volume V, the gas volume corresponding to the initial portion of the chamber up to the position x

As in Eq. (4), we can write

$$W_w = K\rho_w A_w P_g^s \quad (20)$$

Since, by definition, we also have

$$W_g = \rho_g A_g u_g \quad (21)$$

Eq. (19) can be solved for u_g to obtain [with the use of Eq. (5)]:

$$u_g = \frac{K\rho_w R T_g}{A_g P_g^{1-s}} A_w - \frac{1}{A_g P_g}\frac{dP_g}{d\tau} V \qquad 0 \leq x \leq L, \quad \tau > 0 \quad (22)$$

where the coefficients of A_w and V are functions of τ only (because of the assumed uniformity of T_g, P_g, and A_g with x). Thus, we can describe the behavior of u_g as a function of x and τ by examining A_w and V. $\bar{V}$ is a constant since it is assumed that no recession of the grain surface occurs; thus A_g is constant (we already know that A_g is uniform in x) and we can express V as a linear function of x for all τ:

$$V = A_g x \qquad 0 \leq x \leq L, \quad \tau > 0 \quad (23)$$

To examine A_w, it is necessary to consider its behavior in two time periods, $0 \leq \tau < \tau_L$ and $\tau \geq \tau_L$, where τ_L is defined to be the time at which the flame front reaches the end of the grain [i.e., the smallest value of τ which satisfies the equation $\sigma(\tau) = L$]. Clearly $\tau_L < \tau_f$, where τ_f is the time at which the gas pressure P_g reaches a steady-state value. Then, since the inside grain surface area is linear in x, we see that, for τ in $0 \leq \tau < \tau_L$, A_w is linear in the interval $0 \leq x \leq \sigma$ and constant in $\sigma \leq x \leq L$. For $\tau \geq \tau_L$, since $\sigma = L$, we see that A_w is linear in the whole interval, $0 \leq x \leq L$.

Thus, due to Eq. (23) and the piecewise linearity of A_w, we see that each value of τ during flame spreadin g($0 \leq \tau < \tau_L$)u_g, as given by Eq. (22), increases linarly in $0 \leq x \leq \sigma$ from $u_g(0, \tau) = 0$ to the value

$$u_g(\sigma, \tau) = \frac{K\rho_w R T_g}{A_g P_g^{1-s}} A_w(\sigma, \tau) - \frac{1}{A_g P_g}\frac{dP_g}{d\tau} V(\sigma) \quad (24)$$

and then decreases linearly from $u_g(\sigma, \tau)$ to

$$u_g(L, \tau) = \frac{K\rho_w R T_g}{A_g P_g^{1-s}} A_w(\sigma, \tau) - \frac{1}{A_g P_g}\frac{dP_g}{d\tau} V(L) \quad (25)$$

[$u_g(L, \tau) < u_g(\sigma, \tau)$ because $V(L) > V(\sigma)$.] After flame spreading ($\tau \geq \tau_L$), however, u_g increases linearly for each τ over the whole interval $0 \leq x \leq L$ from $u_g(0, \tau) = 0$ to

$$u_g(L, \tau) = \frac{K\rho_w R T_g}{A_g P_g^{1-s}} A_w(L, \tau) - \frac{1}{A_g P_g}\frac{dP_g}{d\tau} V(L) \quad (26)$$

Moreover, despite the time dependence of P_g and $dP_g/d\tau$, it will be shown in a moment that $u_g(L, \tau)$ is constant for all τ. This implies that the distribution for u_g is invariant after flame spreading, since, for $\tau \geq \tau_L$, u_g is a linear function passing through 0 and $u_g(L, \tau)$.

There are several ways of showing that $u_g(L, \tau)$ is independent of τ. For example, by writing a mass balance at $x = L$ we obtain

$$\rho_g A_g u_g(L, \tau) = W_g(L, \tau) = W_n = M'A^*P_g/(T_g)^{1/2} \quad (27)$$

for all τ. Thus

$$u_g(L, \tau) = M'R(T_g)^{1/2}(A^*/A_g) \equiv B \quad (28)$$

for some constant B.

In Fig. 1b the piecewise linear distribution of u for $0 \leq \tau < \tau_L$ is shown for several values of $\sigma < L$, and the limiting steady-state linear distribution is also shown for $\tau \geq \tau_L$. It should be noted that, since τ_f is the time at which P_g reaches a steady-state value (whereas the distribution u_g becomes steady at $\tau = \tau_L$), the pressure will still increase after the end of the flame spreading.

We see in Fig. 1b that, as the flame front proceeds down the grain (i.e., as σ gets larger), $u_{g,\sigma}$ progressively decreases to the limiting value $u_{g,L}$ [this can be proved directly by substituting $dP_g/d\tau$ from Eq. (8) in expressions (25) and (26)].

Recall that the velocity distribution given by Eq. (22) and sketched in Fig. 1b was obtained on the basis of only a mass balance, and the assumed uniform distribution of the chamber pressure and temperature upstream of the nozzle at each instant of time. This implies that momentum effects are being ignored since consideration of a momentum balance would indicate that, over the flaming portion of the wall, the pressure would decrease as x increases. For a uniformly distributed gas temperature the gas density would then also decrease as x increases, and hence the velocity might actually increase with x at a faster rate from $x = 0$ to $x = \sigma$ than shown in Fig. 1b. If we were to consider P_g as a function of x, the values of $\bar{W}_w$ would no longer be given by the simple expression $K\rho_w \bar{A}_w P_g^s$,

and the analysis would be greatly complicated. The results of the present study therefore depend heavily on the assumption of uniform P_g and the implied avoidance of momentum considerations.

Finally, it is of interest to show that the steady-state distribution for u_g, given by Eq. (22) for $\tau \geq \tau_L$ and pictured in Fig. 1b, is consistent at $\tau = \tau_f$ and $x = L$ with the expression given by Eq. (18) for $P_{g,f}$. Since $dP_g/d\tau = 0$ at $\tau = \tau_f$, we obtain from Eq. (22)

$$u_g(L, \tau_f) = \frac{K\rho_w RT_g}{A_g P_{g,f}^{1-s}} A_{w,\max} \tag{29}$$

Equation (28), on the other hand, yields the following expression for $u_g(L, \tau_f)$:

$$u_g(L, \tau_f) = M'R(T_g)^{1/2}(A^*/A_g) \tag{30}$$

Combining Eqs. (29) and (30) with the use of Eq. (12) results in (18).

Pressure and velocity calculations with a nozzle diaphragm

It is of interest to consider the situation in which a diaphragm is used to block the nozzle throat. The actual diaphragm bursting process is complex, and pressure discontinuities may be propagated in the chamber. However, for the present analysis, such phenomena will be ignored, and it will be assumed that the diaphragm ruptures instantaneously.

If a diaphragm is used to block the nozzle throat, then, using a mass balance as before, we have $W_n = 0$ and the first term on the right side of Eq. (8) vanishes yielding

$$K\rho_w \bar{A}_w P_g^s = (\bar{V}/RT_g)(dP_g/d\tau) \tag{31}$$

Letting the value of $\bar{A}_w$ be constant in the time interval $\Delta\tau$ (as before), the Eq. (31) may be integrated over sufficiently small $\Delta\tau$ to give

$$P_{g,\nu} = \left[P_{g,\nu-1}{}^{1-s} + \left(\frac{K\rho_w RT_g \bar{A}_{w,\nu-1}}{\bar{V}} \right)(1-s)\Delta\tau \right]^{1/(1-s)} \qquad \nu = 1, 2, \ldots \tag{32}$$

As long as the diaphragm remains in the nozzle throat, Eq. (32) is used to compute the chamber pressure response. After rupture, Eq. (10) provides the appropriate description of the pressure response as before.

Similarly, $dP_g/d\tau$ is obtained from Eq. (31) before diaphragm rupture and from Eq. (8) afterward. Then, from Eqs. (22) and (31), it can be shown as expected that prior to bursting of the diaphragm

$$u_g(L, \tau) = 0 \tag{33}$$

Hence, before diaphragm rupture, the velocity distribution for each value of τ will increase linearly with x in $0 \leq x \leq \sigma$ and then decrease linearly to zero in $\sigma \leq x \leq L$. (Since the diaphragm will generally burst before the end of flame-spreading, we need not consider the case of $\tau \geq \tau_L$.)

Heat Transfer Calculations

Heat conduction in the grain

As already indicated, the solution for the gas pressure $P_g(\tau)$ is coupled (through the flame-spreading phenomenon and the transfer of heat to the unburned portion of the grain) to a solution of the heat-conduction problem in the grain for the grain temperature.

The parabolic partial differential equation describing the continuous two-dimensional transient distribution of temperatures in the solid grain can be written in the following form:

$$T_\tau(x, y, \tau) = \alpha_a T_{xx}(x, y, \tau) + \alpha_b T_{yy}(x, y, \tau) \qquad 0 \leq x \leq L, \quad 0 \leq y \leq \delta, \quad \tau > 0 \tag{34}$$

where α_a and α_b are the constant thermal diffusivities of the grain in the x and y directions, respectively. The initial and boundary conditions for the problem consist of the following:

Initial Conditions

$$T(x, 0, 0) = \begin{cases} T_{ig} & 0 \leq x \leq \sigma(0) \\ T_I, & \sigma(0) < x \leq L \end{cases}$$

$$T(x, y, 0) = T_I \qquad 0 \leq x \leq L, \quad 0 < y \leq \delta \tag{35}$$

Boundary Conditions

$$T_x(0, y, \tau) = 0 \qquad 0 \leq y \leq \delta, \quad \tau > 0 \tag{36}$$

$$T_x(L, y, \tau) = 0 \qquad 0 \leq y \leq \delta, \quad \tau > 0 \tag{37}$$

$$T_y(x, \delta, \tau) = 0 \qquad 0 \leq x \leq L, \quad \tau > 0 \tag{38}$$

$$T(x, 0, \tau) = T_{ig} \qquad 0 \leq x \leq \sigma(\tau), \quad \tau > 0 \tag{39a}$$

$$-k_b T_y(x, 0, \tau) = h(x, \tau)[T_g - T(x, 0, \tau)] \qquad \sigma(\tau) < x \leq L, \quad \tau > 0 \tag{39b}$$

where T_{ig} is the ignition temperature (constant after ignition), T_g is the constant gas temperature, k_b is the constant thermal conductivity of the grain in the y direction, and $h(x, \tau)$ is the effective heat-transfer coefficient characterizing the transfer of heat to the unignited portion of the wall surface. As before, $\sigma(\tau)$ represents the axial length of the ignited portion of the grain surface at any time τ, i.e., the axial position of the advancing flame front. In general, $\sigma(\tau)$ is not a known function except at $\tau = 0$ and cannot be expressed explicitly in the boundary condition (39b). In a numerical solution of Eq. (34), however, this presents no difficulty, since its position for each time step is automatically located at the last axial mesh point to have been ignited. It is through the coefficient $h(x, \tau)$ that the grain temperature and gas pressure are coupled, since h is directly a function of the Reynolds number which is in turn a function of gas pressure (conversely P_g depends on T through A_w). A more complete discussion of the formulation of h appears below.

The solution of Eqs. (34–39b) is obtained by finite-difference procedures using the alternating-direction method of Peaceman and Rachford[1] for the discretization. The advantages afforded by this method are its numerical stability for any size time step and the tridiagonality of the resulting linear system of algebraic equations, which thereby admit of a direct solution for each time step. Both properties tend to reduce the amount of computing time necessary for the solution.

Heat transfer at the unburned grain surface

In the formulation of the required boundary condition [Eq. (39b)] for describing the heat flux to the unburned surface of the grain, use is made of an axially varying effective heat-transfer coefficient given in the following form:

$$h(x, \tau) = a(k_g/\chi)(\rho_g \chi u_g/\mu)^b (c_{p,g}\mu/k_g)^c + \psi \tag{40}$$

where a, b, and c are constants ($b < 1$) depending on mass diffusion, combustion, and transient boundary-layer effects, and $\chi = x - \sigma$ is distance measured from the flame front. The function ψ, which depends on temperature and pressure, has been introduced formally to describe the effects of radiation from the hot gas and unburned particles, gas phase condensation, and particle impingement upon the grain surface; values of ψ can be estimated experimentally. For purposes of the present analytical program (thus far used only in conjunction with existing experimental data), the function ψ was omitted and, to account for possible effects consequently neglected, the range of the coefficient "a" in Eq. (40) was considerably extended. A more detailed discussion of the effects of the various heating mechanisms contributing to the flux at the grain surface may be found in Ref. 2. However the following brief comments seem pertinent here.

It should be emphasized that Eq. (40) is a crude but convenient expression to represent the boundary conditions at the unburned surface for the present simplified analysis. Following is a list of most of the pertinent phenomena that should be accounted for in a rigorous evaluation of the effective heat-transfer coefficient. Some items in the list have been dealt with in a more or less exact fashion in Eq. (40).

1) The flow in the ports of most solid propellant motors is more akin to the flow in a short pipe than to hydrodynamically developed pipe flow; hence the convective heat-transfer coefficient depends not only on port diameter but is also a function of flow path length in the axial direction.

2) A sharp temperature gradient exists at the grain surface at that axial position separating the burning portion of the grain surface from the unburned portion.

3) The temperature distribution along the unburned grain surface is not uniform.

4) The flow conditions in the port are highly transient.

5) The flow velocity varies both with time and position.

6) Mass ejection with chemical reactions exists over the burning portion of the wall.

7) Gas phase condensation may exist along with exothermic and/or endothermic reactions along the unburned grain surface.

8) The unburned grain surface undergoes pyrolysis.

9) Thermal radiation is emitted by the flowing gases, incandescent particles, and the burning portion of the grain surface to the unburned portion of the grain surface.

10) Incandescent particles may impinge on the unburned grain surface.

Item 1 of the foregoing list suggests a convective heat-transfer model that would be a compromise between the problem solved by Graetz[3] and that solved by Kays.[4] Both of these methods are rather cumbersome and Kays' method is strictly numerical. A sweeping simplification of the complicated phenomena involved in item 1 is suggested in the following statement by Kreith:

> For very short tubes or rectangular ducts with initially uniform velocity and temperature distribution, the flow conditions along the wall approximate those along a flat plate, and the Pohlhausen[6] analysis (for a flat-plate boundary layer) is expected to yield satisfactory results for fluids having Prandtl numbers between 1.0 and 15.0. The Pohlhausen solution applies when L_c/d is less than 0.0048 Re_d for tubes.[5]

In fact some recent experimental work corroborates the flat-plate approximation incorporated in Eq. (40). Davey[10] has reported that the following expression was used successfully to correlate entrance region flow:

$$hD/k_g = a(Re)_D^{0.8}(Pr)^{0.4}(x/D)^d(T_b/T_w)^e \qquad (41)$$

where

D = duct diameter
Re_D = Reynolds number (based on duct diameter)
T_b = bulk temperature of fluid
T_w = inside wall temperature
a, d, e = const

A series of experiments reported in the paper enabled Davey to evaluate the constants a, d, and e as follows: $a = 0.036$, $d = -0.2$, and $e = 0.18$.

His final expression, which gave an excellent correlation, appears as follows:

$$Nu_{\text{local}} = 0.036(Re)_D^{0.8}(Pr)^{0.4}(x/D)^{-0.2}(T_g/T_w)^{0.18} \qquad (42)$$

When multiplied together, the dimensionless parameters Re, Pr, x/D are generally used to express the exact solution to the Graetz problem which, among other things, concerns the convective heat-transfer coefficients in the entrance region of tubes with isothermal walls. Hence, these parameters were used in a modified form by Davey to correlate his experimental data. Equation (42) was not carried any further in the referenced paper, but had it been, the following development would have resulted: since $Nu_{\text{local}} = h_{\text{local}} D/k_g$, it is readily seen that the numerical values in the foregoing equation are such that the D term completely cancels itself out of the expression, and the expression becomes

$$h_{\text{local}}x/k = 0.036(Re_x)^{0.8}(Pr)^{0.4}(T_b/T_w)^{0.18} \qquad (43)$$

The latter expression correlates the convective heat-transfer coefficient for a turbulent boundary layer over a flat plate (Davey used turbulent flow) and, except for the $(T_b/T_w)^{0.18}$ term, is identical in form with the first term on the right-hand side of Eq. (40). The $(T_b/T_w)^{0.18}$ term is simply one of property correction, which need not be used if the other constants are adjusted slightly and a "reference temperature" correction is used instead. Although this verification is valid for the case of isothermal walls, it will be shown in a moment that Eq. (40) can be adapted to the case of nonisothermal surfaces.

There is a great deal of information in the literature regarding the effects of wall temperature gradients and flow velocity gradients on the convective heat-transfer coefficient (items 2–5 of the foregoing list). The errors incurred by ignoring nonuniform surface temperature distributions are more severe for the laminar boundary layer than for the turbulent and depend on the magnitude of the temperature gradients. The methods developed to evaluate these effects are generally cumbersome.

Eckert, Hartnett, and Birkebak[7] have attempted to simplify the procedure required to evaluate effects due to both surface temperature and pressure gradients. They present results, for certain families of flows, in terms of Nu/Nu_{iso} where Nu_{iso} is the Nusselt number for the case of a flat isothermal plate given by

$$Nu_{\text{iso}} = a'(\rho_g x u_g/\mu)^{b'}(c_{p,g}\mu/k_g)^{c'}$$

Comparison of this expression with Eq. (40) reveals the motivation for multiplying a' by a factor Nu/Nu_{iso} to construct the value of the coefficient a in the latter equation.

The velocity variations mentioned in item 5 are spatial variations connected with steady flow problems. The velocity variations during the ignition period in a solid-propellant rocket combustion chamber are further complicated by

Table 1 Input used for results obtained

m	= 26.9
A^*	= 0.0001075 ft^2
A_g	= 0.00434 ft^2
s	= 0.47
K	= 0.0152
T_g	= 5823°R
T_I	= 530°R
k_g	= 1.11×10^{-5} Btu/sec-ft-°F[a]
μ	= 2.78×10^{-5} lb/sec-ft[a]
$c_{p,g}$	= 0.441 Btu/lb-°R
P_I	= 2120 psf
P_{amb}	= 2120 psf
$k_{w,b}$	= 7.4×10^{-5} Btu/sec-ft-°F
c_w	= 0.253 Btu/lb-°R
ρ_w	= 109 lb/ft^3
σ_0	= 0.0916 ft
β	= 0.0417 ft
T_{ig}	= 1500°R
$\bar{V}$	= 0.00253 ft^3
L	= 0.458 ft
γ	= 1.201
b	= 0.5
c	= $\frac{1}{3}$

[a] Since the the thermal conductivity and viscosity of the gas were not known, approximate values for superheated steam were used.

transient phenomena. Effects on heat-transfer coefficients due to transient flows in general are not well known. For the steady flow case, flow decelerations tend to thicken the boundary layer, and flow accelerations tend to retard boundary-layer growth or even thin out the boundary layer. As a rule a thicker boundary layer implies a lower convective heat-transfer coefficient. Well-known schlieren pictures (or smoke pictures) indicate that, at the onset of flow over a body, the boundary layer is not discernible and the entire flow pattern appears inviscid. As time progresses, a boundary layer materializes and thickens with the flow pattern changing from inviscid to viscous. This seems to indicate that friction coefficients are lower and that probably convective heat-transfer coefficients are higher during the transient period than under steady-state conditions.

As a crude approximation for transient effects, the entire flow field may be considered to exist as a "slug flow," i.e., a uniform velocity distribution in the direction normal to the flow. If initially a boundary layer is indeed not discernible, then the slug flow approximation may not be a bad one. Kreith[5] indicates that a slug flow solution for the convective heat-transfer coefficient gives values that are approximately twice the corresponding values for a parabolic velocity distribution. It should be reiterated that these remarks concerning heat-transfer coefficients in a highly transient flow are only speculative. If there is any validity to the previous argument, however, it should be possible to include the effects of many of the mechanisms through the constant a in Eq. (40).

The effect of mass ejection with chemical reactions (item 6) has been treated in the literature (cf. Refs. 8 and 9). The effect on the unburned grain surface near the flame front of the mass ejection from the burning grain surface is difficult to evaluate, however. This mass ejection creates velocity components perpendicular to the main flow and hence has a tendency to reduce convective heat-transfer coefficients in this region.

The analysis of gaseous condensation phenomena (item 7) has been given only limited attention in the literature. Aside from a boundary-layer analysis of filmwise condensation on vertical surfaces, information regarding condensation phenomena is limited to empirical data involving a few specific fluids condensing over horizontal tubes or vertical surfaces. Except for specific numerical data for steam, very little is known about dropwise condensation. Suffice it to say at this point that these effects should be accounted for in the ψ term of Eq. (40) by correlating with experimental results involving ignition for realistic grain configurations. In the absence of such information, we have set $\psi = 0$. The same types of remarks apply to incandescent particle impingement (item 10).

The pyrolysis of the unburned grain surface (item 8) tends to counteract the effect of gaseous condensation and increases the temperature response time of the unburned grain surface.

The thermal radiation effect (item 9) should also be accounted for in the ψ term of Eq. (40), since an "effective radiation heat-transfer coefficient" is temperature dependent because of the fourth power temperature dependence of the radiative heat flux. If at a point on the unburned surface near the flame front, the configuration factor (or geometric factor) is assumed to be roughly one-half for the radiation emitted from the burning portion of the wall, and if gaseous and incandescent particle radiation is considered (tending to increase the configuration factor closer to unity), then a rough calculation indicates that the radiative heat flux is significant. It is possible to compute such configuration factors accurately, but more difficult to accurately determine temperature levels and size distribution of the incandescent particles. Aside from such common gases as carbon dioxide, water vapor, methane, and carbon monoxide, the emissivities or absorption coefficients of other radiating species are difficult to assess. It is hoped to include explicitly some of the real factors influencing surface heat transfer discussed here in future extensions of the present analysis.

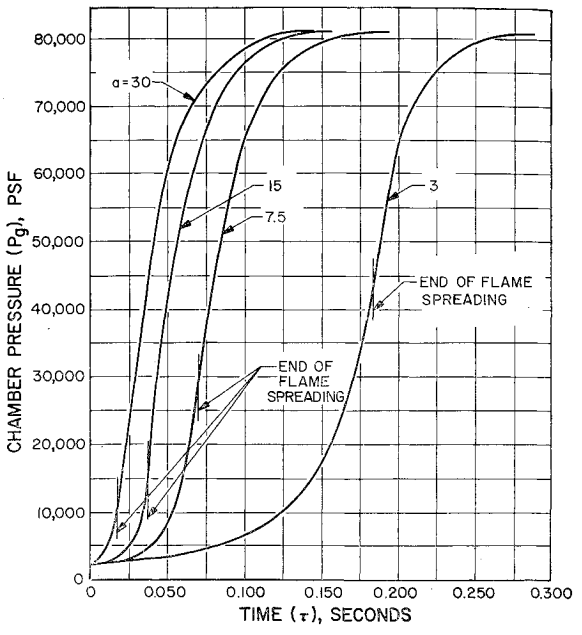

Fig. 2 Pressure response without diaphragm ($P_{burst} = 0$) for coefficients $a = 30$, 15, 7.5, and 3. (The single curve for $a = 30$ depicts the response for both $k_{w,a} = 0$ and $k_{w,a} = k_{w,b}$).

Results and Discussion

A computer program was written for the Rocketdyne IBM 7094 to perform the complete coupled analysis already presented. The output includes a visual display (cathode ray tube) of the pressure history from $\tau = 0$ to $\tau = \tau_f$. All numerical results thus far obtained have as basic input the numerical data listed in Table 1. Differing results were obtained by varying coefficient a of Eq. (40) and through use of the two following program options: 1) the axial grain conductivity $k_{w,a}$ (one of the input parameters) can be set either equal to 0 or to $k_{w,b}$ in order to obtain one-dimensional or two-dimensional conduction analyses in the grain, and 2) the (input) value of diaphragm burst pressure can be made greater than or less than the initial pressure of the chamber in order to simulate ignition with or without diaphragm.

The resulting graphs of P_g as a function of τ are shown in Figs. 2 and 3. Option 1 was exercised only for the single value $a = 30$, since the difference in the results obtained proved to be negligible. Thus the single curve for $a = 30$ in Fig. 2 represents both the alternatives of option 1. It would appear (at least for the input data given in Table 1) that longitudinal heat conduction effects at the grain surface even near the flame front are negligible. For the remaining computer runs, $k_{w,a}$ was always taken to be zero.

The effect of differing rates of heat transfer to the unburned grain surface (i.e., differing values of the coefficient a) is shown in Fig. 2 for the case of ignition without a diaphragm and in Fig. 3 for ignition with a diaphragm (assuming a diaphragm burst pressure of 40,000 psf). The difference in the curves obtained with a diaphragm (at $P_{burst} = 40{,}000$ psf) and without a diaphragm can be observed by a comparison of Figs. 2 and 3 for $a = 3$ and 7.5. Finally, Fig. 3 contrasts the effects of differing values of P_{burst} (40,000 and 20,000 psf) with a diaphragm present for the case $a = 3$.

The response to the rupture of the diaphragm is shown to occur instantaneously in Fig. 3. Actually, a finite time increment is necessary for diaphragm rupture, and there is no real discontinuity in the first derivative of pressure with respect to time. (Under certain conditions measurable pressure fluctuations due to shock and rarefaction waves would be superimposed on the pressure response curve in the region of dia-

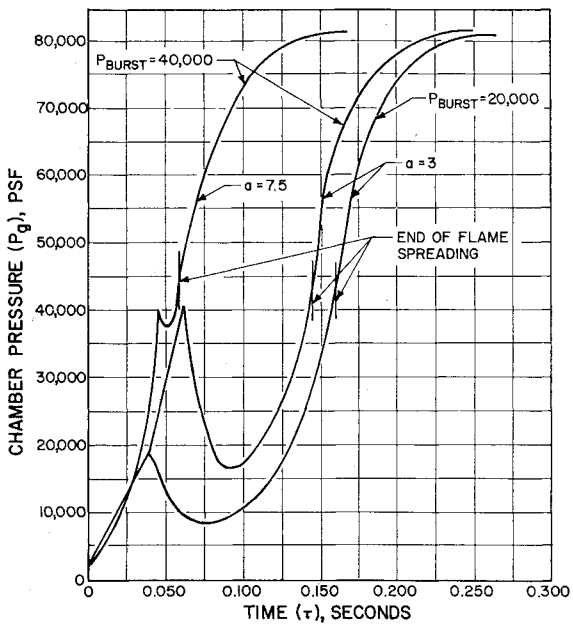

Fig. 3 Pressure response with diaphragm for differing values of a and P_{burst}.

phragm rupture due to wave reflections just after the time of diaphragm rupture. As pointed out earlier, the one-dimensional approach used here does not account for these effects.)

In Fig. 3, furthermore, there appears to be an inconsistency; this, however, is only apparent and does not reflect errors in the calculation procedure. In each of the curves for $a = 3$, the first part ($0 \leq \tau < 0.0356$) is pictured as a straight line whose curvature does not conform to its extension ($\tau > 0.0356$). This results directly from the method employed in the machine program for selecting values of pressure to be plotted on the CRT graphs (of which Figs. 2 and 3 are duplicates). The values plotted were chosen when and only when an axial mesh point reached ignition temperature. For $a = 3$ and $P_{burst} = 20{,}000$ or $40{,}000$, however, the flame spreading at first was slow and was accompanied by a rapid pressure rise. This, combined with the fact that the CRT plotter always uses straight line interpolation between points plotted, caused the apparent discrepancies in the curves. In Fig. 3, for $P_{burst} = 20{,}000$, it can be seen for example that, by the time the first new axial point had been ignited, the pressure had already reached burst value and was descending. Actually many intervening values of pressure were computed (and printed out) during the machine calculation. The graphs have not been corrected for publication, however, since the machine program has not yet been adjusted to plot as well as to print the missing values. The authors feel that possible users of the programs prior to its adjustment would be misled by the CRT output were it inconsistent with the graphs presented here.

It can also be seen in Fig. 3, for $P_{burst} = 40{,}000$, that the value plotted at the time of diaphragm rupture in each case exceeds burst pressure. This does reflect an error in the machine calculation which can easily be corrected in the program by reducing the calculated pressure to the value of P_{burst} at the time of rupture. In any case, the error is slight for a small enough time step.

It is interesting to consider alternate sets of initial values. For example, suppose it were assumed that the length of the initially ignited portion of the grain were significantly smaller. Then the criteria expressed by inequalities (15) and (16) for the case of no nozzle diaphragm would imply that the chamber pressure would at first decrease below its initial value. This situation leads to difficulties if the initial chamber pressure is equal to the ambient pressure P_{amb}, for then inequality (16) implies that $P_g < P_{amb}$ immediately after time 0, an impossible situation. This difficulty arises because of the use of Eq. (6) to express the gas efflux rate through the nozzle even during the earliest stages of ignition when the nozzle is not choked. During this brief period, the assumption of choked flow breaks down, although it is valid shortly after ignition because of the rapid rise of chamber pressure. During the unchoked period of operation, far more complicated expressions would be required to describe the gas-efflux rate. It is important to insure against this erroneous inequality $P_g < P_{amb}$, since heat-transfer calculations based on such falsely low pressure (when actually $P_g \cong P_{amb}$) would lead to the computation of an erroneously low flame-spreading rate and consequently to the prediction of a "hang fire" (i.e., no significant flame spreading). To avoid such a situation, each value of P_g computed in the program is compared to the ambient pressure, and if less, P_g is replaced by P_{amb} (only for the calculation of gas density). It is felt that this simplification in the computation procedure does not significantly affect the transient pressure response time.

The foregoing remarks do not of course imply that a hang fire cannot occur. A hang fire can physically result if a sufficiently small grain surface area is initially ignited and, in addition, if heat-transfer effects are not large enough to spread the flame significantly within a short enough period of time. This could occur, for example, in the case of a very low initial chamber pressure, no diaphragm, and a sufficiently small heat-transfer rate to the grain surface.

References

[1] Peaceman, D. W. and Rachford, H. H., Jr., "The numerical solution of parabolic and elliptic differential equations," J. Soc. Ind. Appl. Math. **3**, 28–41 (March 1955).

[2] deSoto, S., "Some elementary considerations regarding heat transfer to solid grain propellants during the ignition process," Rocketdyne Research Memo. 940–351 (July 1963).

[3] Graetz, L., "Uber die Warmeleitungsfahigkeit von flussigkeiten," Anal. Physik Chem. **25**, 337–357 (1885).

[4] Kays, W. M., "Numerical solutions for laminar flow heat transfer in circular tubes," Trans. Am. Soc. Mech. Engrs. **77**, 1265–1274 (1955).

[5] Kreith, F., *Principles of Heat Transfer* (International Textbook Co., Scranton, Pa., 1958), p. 358.

[6] Pohlhausen, E., "Der Warmeaustausch zwischen festen Korpern und Flussigkeiten mit kleiner Reibung und kleiner Warmeleitung," Z. Angew. Math. Mekh. **I**, 115 (1921).

[7] Eckert, E. R. G., Hartnett, J. P., and Birkebak, R., J., "Simplified equations for calculating local and total heat flux to nonisothermal surfaces," Aeronaut. Sci. **24**, 549–550 (1957).

[8] Hartnett, J. P. and Eckert, E. R. G., "Mass transfer cooling with combustion in a laminar boundary layer," *Proceedings of the 1958 Heat Transfer and Fluid Mechanics Institute* (Stanford University Press, Stanford, Calif., 1958).

[9] Lees, L., "Convective heat transfer with mass addition and chemical reactions," *Combustion and Propulsion, Third AGARD Colloquium* (Pergamon Press, New York, 1958), pp. 451–498.

[10] Davey, T. B., "Entrance region heat transfer coefficients," Heat Transfer **59**, 47–51 (1963).